

ORIGINAL ARTICLE

Open Access



# Corrosion behavior of AlCrVTi light-weight high-entropy alloy coating in different corrosion environments

Bowei Xing<sup>1</sup>, Sainan Nie<sup>1</sup>, Bingqian Jin<sup>1</sup>, Xiaojiao Zuo<sup>1</sup>, Huishu Yu<sup>1</sup>, Xin Wang<sup>1</sup>, Xu Zhang<sup>1</sup> and Nannan Zhang<sup>1\*</sup>

## Abstract

The excellent corrosion resistance of high-entropy alloys (HEAs) has attracted widespread attention in recent years. The focus of research is gradually shifting from the performance characterization to the composition design and application that balance multiple performance. In this study, the AlCrVTi light-weight HEA has been chosen to investigate the corrosion behavior in the electrochemical and salt spray environment. The results show that HEA coating prepared by plasma spray followed laser re-melting present a homogeneous single-phase microstructure. The active Ti and V elements promote the formation of passive film during corrosion, which improves the corrosion resistance of HEA coating. Therefore, the HEA presents a higher corrosion resistance compared with 304 stainless steel (SS304), which is reflected in the lower corrosion current density. In the salt spray environment, the coating still presents the pitting corrosion, which is same as in the electrochemical environments. It is demonstrated that the AlCrVTi HEA has the potential that balancing the corrosion resistance and mechanical properties.

**Keywords** AlCrVTi high-entropy alloy, Plasma spray, Laser re-melting, Corrosion resistance, Salt spray corrosion

## 1 Introduction

The research on the corrosion resistance of HEAs is rapidly developing, and a large number of reports and outstanding work have emerged [1–5]. HEAs, also known as multi-principle element alloys (MPEAs), is a popular alloy design concept [6]. Its unique multi-principle element feature, as well as the concomitant high-entropy, lattice distortion, sluggish diffusion, and “cocktail” effects, bring a more homogeneous microstructure, slower dynamics, and synergistic effects between elements, which is benefit to improve corrosion resistance [7]. There are two main systems of corrosion-resistant HEAs, transition metal HEA represented by CoCrFeNi [8, 9] and lightweight

HEA represented by AlCrVTi [10]. Other elements are also used in composition design, transition metal represented by Mo and Mn [11–13], and non-metallic element represented by Si [14]. The AlCrVTi has been confirmed that have excellent mechanical properties [15, 16], which can be applied to industrial production. However, the environment such as oxidation or corrosion in the practical applications should also be considered for protection. Therefore, the corrosion resistance of AlCrVTi HEA should be investigated, especially in the specific corrosion environment. On the other hand, an effective processing method should be developed to prepare the HEA with high performance.

Currently, some methods have been carried out to prepare the HEA. Fu et al. [17] prepared FeCoCrNiAl<sub>0.3</sub> HEA by vacuum arc melting. The HEA shows a higher corrosion resistance than the SS 304. However, with the addition of the Al element, numerous twin boundaries appear on the surface, inducing the pitting corrosion. Xu et al.

\*Correspondence:

Nannan Zhang  
zhangnn@sut.edu.cn

<sup>1</sup> Department of Material Science and Engineering, Shenyang University of Technology, Shenyang 110870, China

[18] prepared CoCrFeMnNi HEA with a more uniform microstructure by selective laser melting (SLM). The SLMed HEA has the lower corrosion current density and the more noble corrosion potential, compared with the as-cast HEA. However, there are some processing defects on the working surface. In these studies, some common patterns were found, where the element segregation and grain boundaries greatly affect the corrosion resistance of the alloy. Meanwhile, the cost, efficiency, convenience, and other factors of processing method should also be considered. In our previous study, the plasma spray has been demonstrated as a feasible method [19]. However, there are some defects and oxides on the sprayed coating surface, which damaged the corrosion resistance. To approach this problem, a laser assisted re-melting is employed to form a more homogeneous surface. As confirmed by Jin et al. [20], the laser re-melting is an effective method to solve the defects on the surface and in-flight oxidation of the coatings. In addition, the performance of the HEA coatings in the specific corrosion environment other than electrochemical system is lacking in reports.

To sum up, in this work, we investigate the corrosion behavior of the plasma sprayed AlCrVTi HEA coating in 3.5 wt.% NaCl solution, 0.5 M H<sub>2</sub>SO<sub>4</sub> solution, 0.5 M HCl solution, and 3.5 wt.% NaCl salt spray environment. The microstructure of the HEA coating and post-corrosion surface are characterized. The present work thus unmasks a high-performance HEA system, which may further develop to the industrial applications.

## 2 Experimental

### 2.1 Materials and preparation

The plasma spraying was carried out to prepare the AlCrVTi HEA coatings, wherein the feedstock powder was synthesized by atomization method. After spraying, the laser re-melting was carried out to optimize the microstructure. The parameters of the spraying and re-melting are listed in Table 1. The samples were cut into a 10 mm×10 mm working surface with a thickness of 2 mm and were polished to 5000# with the silicon carbide paper for the subsequent characterization and tests.

### 2.2 Characterization method

Microstructure was analyzed by field emission scanning electron microscope (FESEM, ZEISS EVO 10), equipped

with energy dispersive spectroscopy (EDS). The phase composition was detected by X-ray diffraction (XRD, Shimadzu 7000) with Cu K $\alpha$  radiation, wherein the scanning angle is 20–100° and the scanning rate is 8°/min.

### 2.3 Electrochemical tests

The electrochemical tests were performed on a Chi604e workstation at room temperature. The three-electrode system was employed, which the sample was the working electrode, the Pt sheet (10×10 mm) was the counter electrode, and the saturated calomel electrode (SCE) was the reference electrode. The working electrodes are hand-making, with the back of the working surface connected to a copper wire and then sealed with epoxy resin. All the tests are repeated at least three times to ensure the accuracy.

Prior to the tests, an open circuit potential (OCP) was recorded after the electrochemical systems reached stabilization, at least 3600 s. The electrochemical impedance spectroscopy (EIS) tests were performed at a frequency range of 100 kHz~10 mHz and a amplitude of 10 mV. The potentiodynamic polarization tests were performed at a potentials range from -0.25 V vs. OCP to the final potential corresponding to a current density of 1 mA/cm<sup>2</sup>, and the scanning rate is 1 mV/s.

### 2.4 Salt spray corrosion and immersion tests

Neuter salt spray tests were carried out in YWX/Q-150 salt spray machine in 3.5 wt.% NaCl solution. The pH value is 6.5~7.2, the temperature is 33~35 °C, and the spray volume is 1.5 ml/(cm<sup>2</sup>·h). The immersion tests were carried out in 0.5 M H<sub>2</sub>SO<sub>4</sub> and 0.5 M HCl solution for 150 h.

## 3 Results and discussion

### 3.1 Bulk properties of HEA coating

Figure 1a and b show the surface and cross-sectional morphology of the AlCrVTi HEA coating, respectively. The coating is compact with a thickness of about 878  $\mu$ m. There are no obvious pore or defect on the surface. Each element in the alloy compose in nearly equal molar ratios and distribute uniformly. In particular, the content of O elements is about 10.79 at. %, which originate from the in-flight oxidation during spraying [21]. As shown in Fig. 1c, the alloy presents a single bcc phase,

**Table 1** Operation parameters of atmospheric plasma spraying and laser remelting

	Working current, A	Wording voltage, V	Protective gas, psi	Powder feed rate, g/min	Scanning speed, mm/min	Working distance, mm	Lapping rate, %
APS	650	40	50	54	2000	150	-
Remelting	100	20	50	-	420	10	30

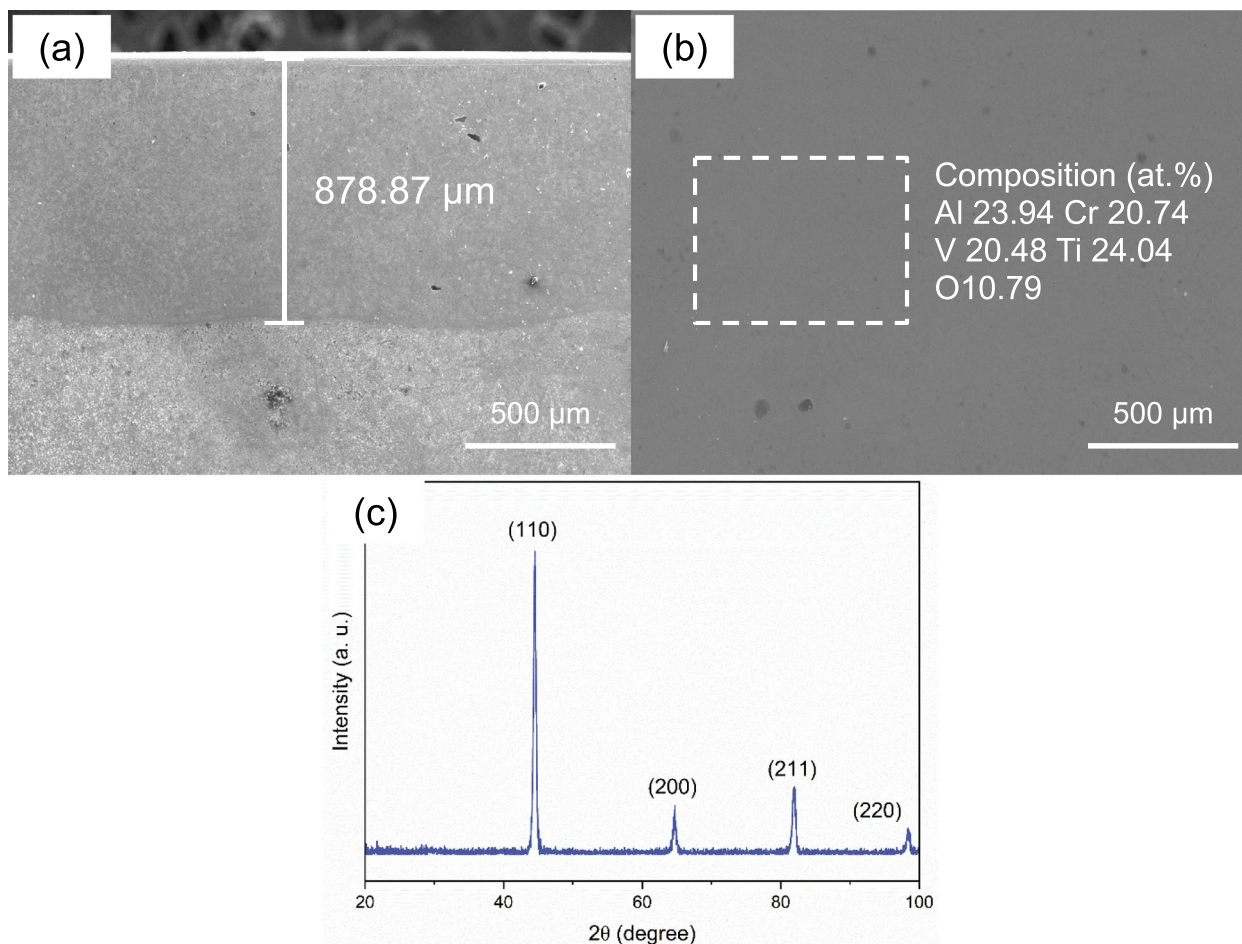


**Fig. 1** The bulk properties of the AlCrVTi HEA coating, **(a)** the cross-sectional morphology, **(b)** the morphology and composition of the surface, **(c)** the phase composition of the surface

corresponding to the (110), (200), (211), and (220) crystal plane. This homogeneous microstructure without elemental segregation and second phase is expected to avoid the galvanic and pitting corrosion.

### 3.2 Electrochemical corrosion behavior of HEA coating

Figure 2 shows corrosion behavior of HEA coating and 304 stainless steel (SS304, as a control) in three different corrosion environment. In all three solutions, HEA exhibits the lower corrosion current density corresponding the higher corrosion resistance, the specific parameter is shown in Table 2. Meanwhile, the more negative corrosion potential of HEA is attributed to the activity of the Al and Ti elements, which makes it easier to form a passive film on the surface. The HEA coating passivates spontaneously when the applied potential noble than the corrosion potential. The passive film constructed of the oxides provides the higher corrosion resistance than the alloy itself, which can be confirmed in EIS results. Taking the results in NaCl solution as an

example, the equivalent circuit can be fitted in three parts, including solution resistance ( $R_s$ ), passive film resistance ( $R_f$ ), and charge transfer resistance ( $R_{ct}$ ), corresponding to the part of solution, passive film, and double layer, respectively. As shown in Table 3, the passive film contributes the largest impedance among these three parts. And the impedance of the passive film formed on the surface of the HEA coating is larger than that on the surface of SS304. Figure 2d and e, the Nyquist and Bode plots, also revealed the larger impedance of HEA coating corresponding to the larger radius of capacitance arc and impedance modulus.

Figure 3 shows the post-corrosion morphology of the HEA coatings. The pitting corrosion present in all three corrosion environment, and is more severe in acidic environment. The corrosion is most severe in 0.5 M HCl solution, that expanding from pitting to strip-shaped corrosion pits. There is a small amount of oxide products on the corrosion surface, corresponding to

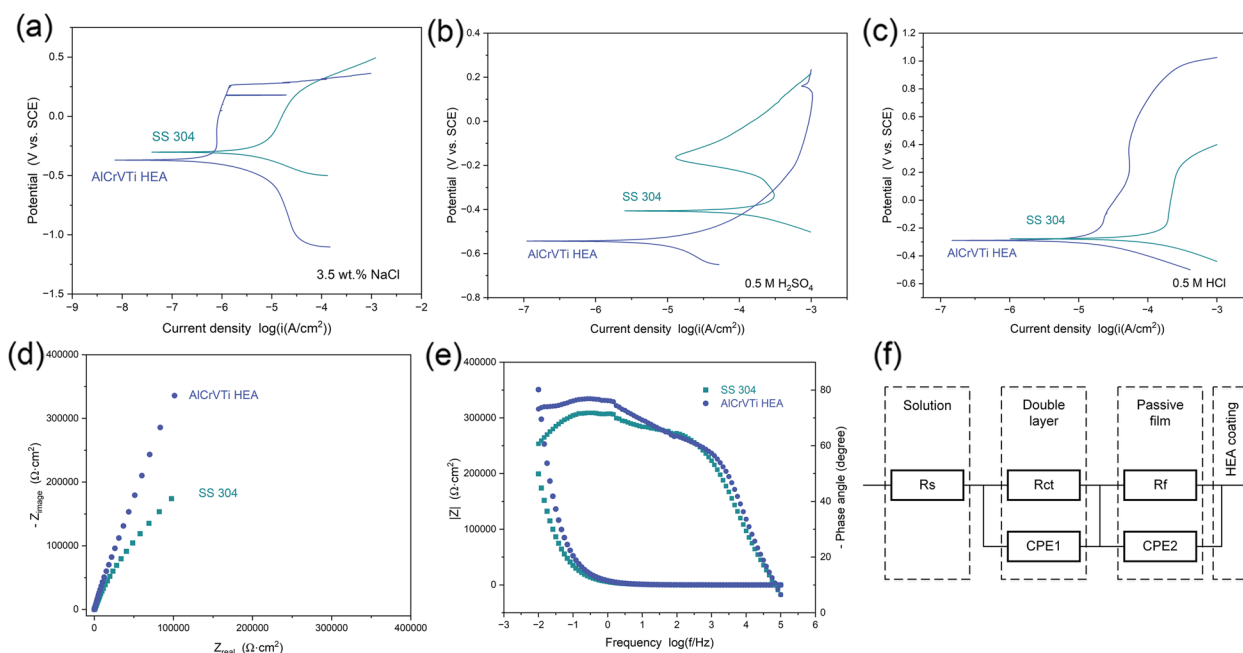


**Fig. 2** Electrochemical corrosion behavior of the AICrTi HEA coating and SS304 in different corrosion environment. The potentiodynamic polarization curves tested (a) in the 3.5 wt. % NaCl solution, (b) in the 0.5 M H<sub>2</sub>SO<sub>4</sub> solution, (c) in the 0.5 M HCl solution, EIS tested in the 3.5 wt. % NaCl solution (d) the Nyquist plot, (e) the Bode plot, and (f) the equivalent circuit

**Table 2** The corrosion current density ( $i_{corr}$ ) and corrosion potential ( $P_{corr}$ ) fitted from potentiodynamic polarization curves

	3.5 wt.% NaCl		0.5 M H <sub>2</sub> SO <sub>4</sub>		0.5 M HCl	
	HEA	SS304	HEA	SS304	HEA	SS304
$i_{corr}$ (A/cm <sup>2</sup> )	$1.023 \times 10^{-7}$	$9.772 \times 10^{-7}$	$3.945 \times 10^{-6}$	$2.512 \times 10^{-5}$	$3.162 \times 10^{-6}$	$2.630 \times 10^{-5}$
$P_{corr}$ (V <sub>SCE</sub> )	-0.365	-0.297	-0.540	-0.404	-0.285	-0.274

**Table 3** The EIS fitted parameters of HEA and SS 304

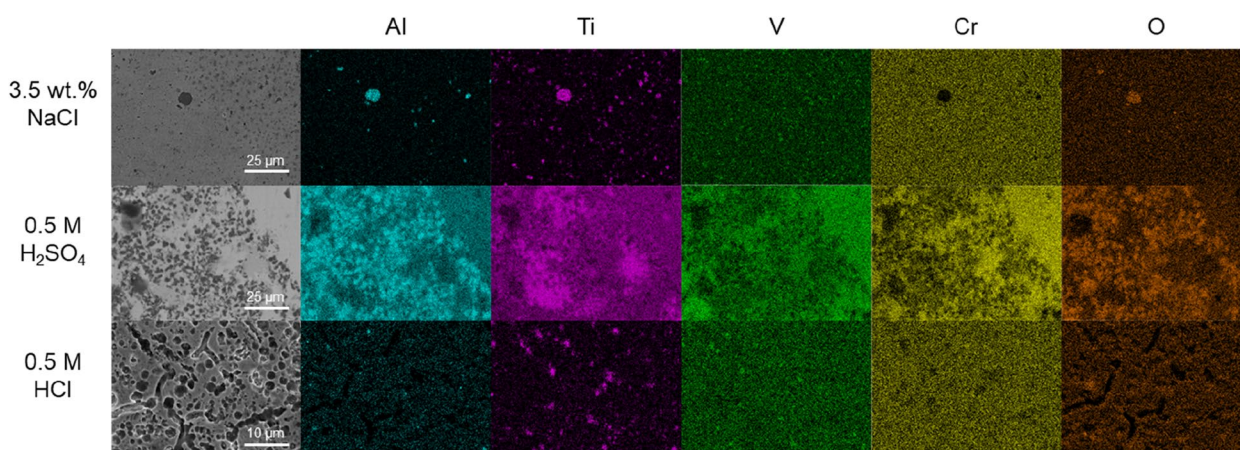
	$R_s$ (Ω·cm <sup>2</sup> )	$R_{ct}$ (Ω·cm <sup>2</sup> )	$R_f$ (Ω·cm <sup>2</sup> )	$CPE1$ (μF·cm <sup>-2</sup> )	$CPE2$ (μF·cm <sup>-2</sup> )	n1	n2
HEA	10.41	$2.75 \times 10^5$	$4.19 \times 10^5$	55.8	32.1	0.51	0.80
SS304	9.68	$1.97 \times 10^5$	$2.82 \times 10^5$	47.3	47.5	0.64	0.77

the segregation of Ti and Al elements and the increase of O element content detected by EDS.

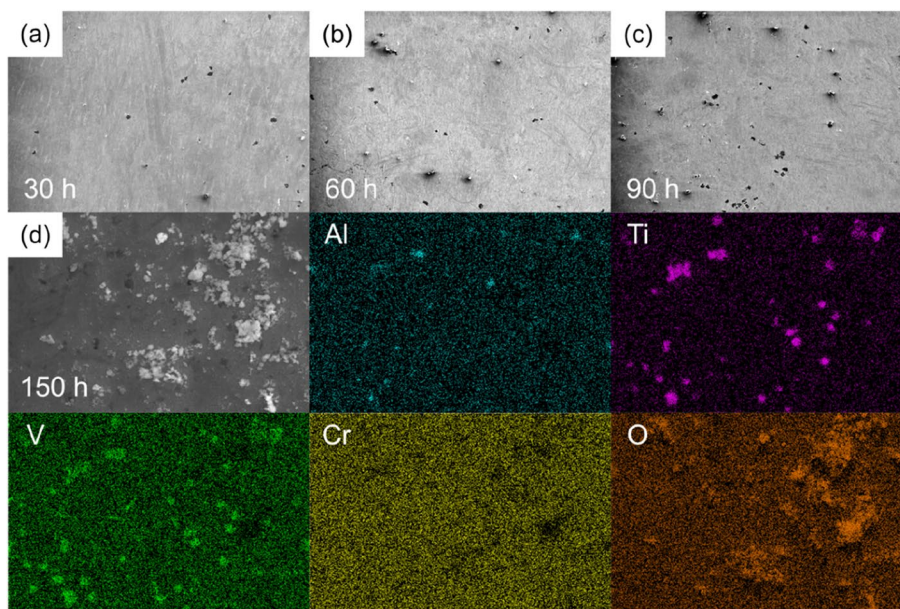
### 3.3 Corrosion behavior of HEA coating in the salt spray environment

Figure 4 shows the morphology of post-corrosion surface in the salt spray environment. The pitting presents on the surface after about 30 h of corrosion. As the corrosion

time increased, the number of pitting continued to increase. After the corrosion time approaches 150 h, a large number of oxidation products presented on the corrosion surface. As shown in the mapping analysis, the corrosion products are more complex compared with the electrochemical corrosion. There is only a small amount of Ti and Al oxides that are similar to electrochemical corrosion. More importantly, the oxides of V and V-Ti



**Fig. 3** Post-corrosion surface of the HEA coatings in different corrosion environment



**Fig. 4** The surface morphology of the HEA coating after (a) 30 h, (b) 60 h, (c) 90 h, and (d) 150 h salt spray corrosion

elements appeared on the corrosion surface. These oxides may form galvanic corrosion with the HEA coating, which may cause further corrosion. However, as mentioned earlier, the uniform oxidation film provides the high corrosion resistance. Therefore, avoiding the segregation of the oxides plays a key role in optimizing corrosion resistance, wherein the high-entropy effect makes the major contributions.

Figure 5 shows the weightlessness curves of the AlCrVTi HEA during the salt spray corrosion. The corrosion rate firstly increases and then decreases, corresponding to

the dissolution and deposition process during the formation of the passive film, respectively. It is demonstrated that the passive film formed after about 60 h corrosion in the salt spray environment. As the corrosion beginning, the alloying elements, especially the active Al and Ti elements, dissolved in the electrolyte. Then, the content of this metal cations in the electrolyte increases gradually, until it exceeds the solubility. Finally, these metal cations deposit on the corrosion surface in the form of oxides and hydroxides, which can improve the corrosion resistance significantly.

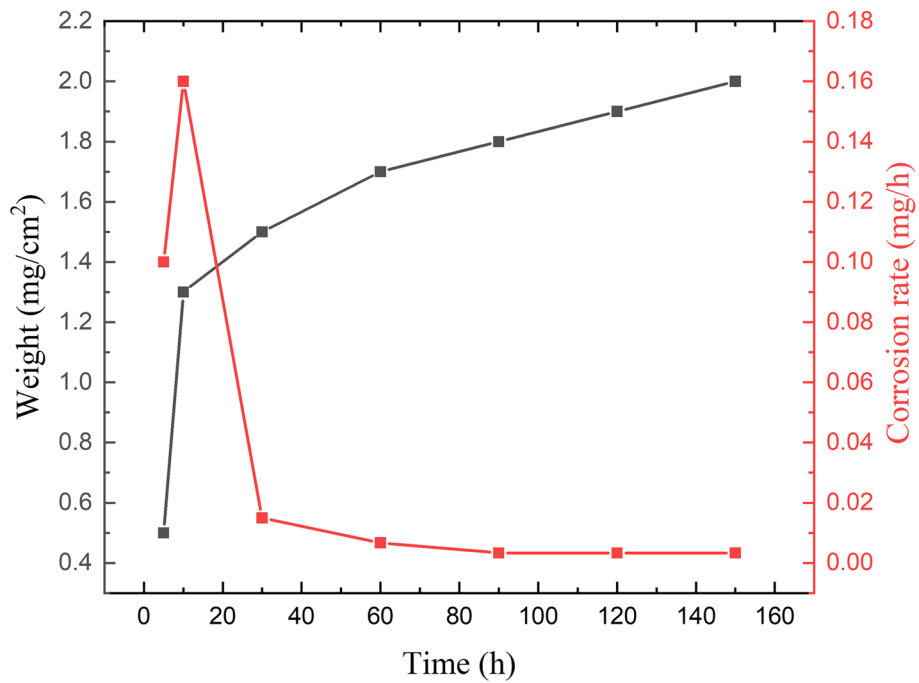


**Fig. 5** The weight loss of the AlCrVTi HEA during the salt spray corrosion

### 3.4 Immersion corrosion behavior in the acidic environment

Immersion corrosion is employed to simulate the corrosion behavior of coatings in real service environment and confirm the corrosion mechanism inferred previously. Figure 6 shows the post-corrosion morphology

of the HEA coating in two acidic solutions, and the composition detected from the enlarged image are listed in Table 4. There are a large number of the corrosion products on the post-corrosion surface in the 0.5 M H<sub>2</sub>SO<sub>4</sub> solution. In the enlarged image, these oxides are loose and porous and may be a damaged

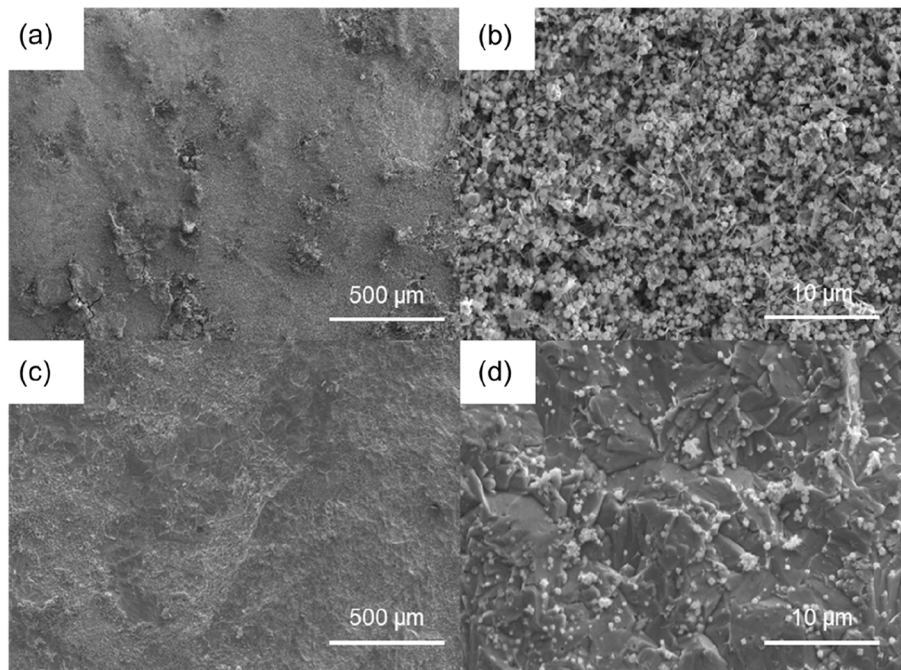


**Fig. 6** The post-corrosion morphology of the HEA coating in (a) (b) the 0.5 M H<sub>2</sub>SO<sub>4</sub> solution and (c) (d) 0.5 M HCl solution

**Table 4** The composition of the post-corrosion morphology of the HEA coating (at. %)

	Al	Ti	V	Cr	O	Fe
H <sub>2</sub> SO <sub>4</sub>	2.75	21.04	36.78	3.13	33.26	3.04
HCl	1.29	3.03	10.11	12.41	5.42	67.74

passive film. As a contrast, the coating in the 0.5 M HCl solution is attached a little corrosion product and contains a large number of Fe element, which is attributed to the dissolution of the coating and the exposure of the Q235 substrate. This phenomenon of generating more oxides in sulfuric acid and more severe corrosion in hydrochloric acid is the same as the results of electrochemical tests.

#### 4 Conclusion

The AlCrVTi HEA coating with a thickness of about 878.87  $\mu\text{m}$  was prepared by plasma spray followed laser re-melting. The HEA coating presents a typical single bcc phase and a homogeneous microstructure without element segregation and second phase. The corrosion current density of the HEA coating in the 3.5 wt.% NaCl, 0.5 M H<sub>2</sub>SO<sub>4</sub>, and 0.5 M HCl solution is  $1.023 \times 10^{-7}$  A/cm<sup>2</sup>,  $3.945 \times 10^{-6}$  A/cm<sup>2</sup>, and  $3.162 \times 10^{-6}$  A/cm<sup>2</sup>, respectively, which is lower than that of the SS304 in the same solution. This higher corrosion resistance is attributed to the formation of passive film with the highest impedance between the electrochemical system. The impedance modulus of the passive film formed on the HEA is  $4.19 \times 10^{-5}$   $\Omega \cdot \text{cm}^2$ , which is larger than that formed on the SS304,  $2.82 \times 10^{-5}$   $\Omega \cdot \text{cm}^2$ . The coating mainly presents pitting after electrochemical and salt spray corrosion. The oxides present on the corrosion surface that composed of Ti and V elements, which causes the galvanic corrosion with the alloy. Therefore, the homogeneous microstructure induced by high-entropy effect plays an important role in improving corrosion resistance.

#### Authors' contributions

Bowei Xing: Data curation, formal analysis, and writing. Sainan Nie, Bingqian Jin, and Xu Zhang: Investigation. Xiaojiao Zuo, Huishu Yu, and Xin Wang: Resources. Nannan Zhang: Methodology, Validation, and Supervision.

#### Funding

This work was supported by Scientific Research Funding Project of the Education Department of Liaoning Province [LJKMZ20220463], Natural Science Foundation of Liaoning Province [2022-MS-272].

#### Availability of data and materials

Data will be made available on reasonable request.

#### Declarations

##### Competing interests

The authors declare that they have no known competing financial interests or personal relationships that could have appeared to influence the work reported in this article. All authors declare that there are no competing interests.

Received: 10 October 2023 Revised: 16 November 2023 Accepted: 19 November 2023

Published online: 06 December 2023

#### References

- Girish KR, Sarathkumar K, Mayank KS et al (2023) A detailed investigation regarding the corrosion and electrocatalytic performance of Fe-Co-Ni-Cr-V high entropy alloy. *Electrochimica Acta* 460:142582. <https://doi.org/10.1016/j.electacta.2023.142582>
- Wang Z, Liu ZX, Jin J et al (2023) Selective corrosion mechanism of CoCrFeMoNi high-entropy alloy in the transpassive region based on the passive film characterization by ToF-SIMS. *Corros Sci* 218:111206. <https://doi.org/10.1016/j.corsci.2023.111206>
- Yao JY, Leandro BS, Sydney FS, et al (2021) Microstructure and corrosion behavior of the Ti-V-Cr-Nb high-entropy alloys in 3.5 wt% NaCl solution. *Corrosion Sci* 218: 111149. <https://doi.org/10.1016/j.corsci.2023.111149>
- Li RX, Kong DH, He KT et al (2023) Improved passivation ability via tuning dislocation cell substructures for FeCoCrNiMn high-entropy alloy fabricated by laser powder bed fusion. *Appl Surf Sci* 621:156856. <https://doi.org/10.1016/j.apsusc.2023.156856>
- Wang JK, Chen YS, Zhang YH et al (2022) Microstructure evolution and acid corrosion behavior of CoCrFeNiCu<sub>1-x</sub>Mo<sub>x</sub> high-entropy alloy coatings fabricated by coaxial direct laser deposition. *Corros Sci* 198:110108. <https://doi.org/10.1016/j.corsci.2022.110108>
- Dworschaka D, Tseng KK, Yeh JW et al (2022) Bottom-up characterization of electrochemical passivity from simple binary alloys to high entropy alloys. *Electrochimica Acta* 405:139804. <https://doi.org/10.1016/j.electacta.2021.139804>
- Fu Y, Li J, Luo H et al (2021) Recent advances on environmental corrosion behavior and mechanism of high-entropy alloys. *J Mater Sci Technol* 80:217–233. <https://doi.org/10.1016/j.jmst.2020.11.044>
- Ana MZ, Alberto MJ, Gisele FLA et al (2023) Corrosion behavior of AlCo-CrFeNi high entropy alloys. *Electrochimica Acta* 441:141844. <https://doi.org/10.1016/j.electacta.2023.141844>
- Shang CY, Axinte E, Ge WJ et al (2017) High-entropy alloy coatings with excellent mechanical, corrosion resistance and magnetic properties prepared by mechanical alloying and hot pressing sintering. *Surfaces and interfaces* 9:36–43. <https://doi.org/10.1016/j.surfin.2017.06.012>
- Qiu Y, Thomas S, Gibson MA et al (2018) Microstructure and corrosion properties of the low-density single-phase compositionally complex alloy AlTiVCr. *Corros Sci* 133:386–396. <https://doi.org/10.1016/j.corsci.2018.01.035>
- Zhao Q, Huang X, Zhan ZX et al (2023) Effect of alloying elements (Mn, Ti, and Mo) on the corrosion behavior of FeCoNiCr-based high entropy alloy in supercritical water. *Corros Sci* 220:111291. <https://doi.org/10.1016/j.corsci.2023.111291>
- Feng H, Li HB, Dai J et al (2022) Why CoCrFeMnNi HEA could not passivate in chloride solution? – A novel strategy to significantly improve corrosion resistance of CoCrFeMnNi HEA by N-alloying. *Corros Sci* 204:110396. <https://doi.org/10.1016/j.corsci.2022.110396>

13. Wang Z, Jin J, Zhang GH et al (2022) Effect of temperature on the passive film structure and corrosion performance of CoCrFeMoNi high-entropy alloy. *Corros Sci* 208:110661. <https://doi.org/10.1016/j.corsci.2022.110661>
14. Zheng SJ, Cai ZB, Pu JB et al (2021) Passivation behavior of VAlTiCrSi amorphous high-entropy alloy film with a high corrosion-resistance in artificial sea water. *Appl Surf Sci* 542:148520. <https://doi.org/10.1016/j.apsusc.2020.148520>
15. Qiu Y, Hu YJ, Taylor A et al (2017) A lightweight single-phase AlTiVCr compositionally complex alloy. *Acta Mater* 123:115–124. <https://doi.org/10.1016/j.actamat.2016.10.037>
16. Feng CS, Feng XB, Guo Z et al (2022) Nanocrystalline (AlTiVCr)N multi-component nitride thin films with superior mechanical performance. *Nanomaterials* 12:2722. <https://doi.org/10.3390/nano12152722>
17. Fu Y, Dai CD, Luo H et al (2021) The corrosion behavior and film properties of Al-containing high-entropy alloys in acidic solutions. *Appl Surf Sci* 560:149854. <https://doi.org/10.1016/j.apsusc.2021.149854>
18. Xu ZL, Zhang H, Du XJ et al (2020) Corrosion resistance enhancement of CoCrFeMnNi high-entropy alloy fabricated by additive manufacturing. *Corros Sci* 177:108954. <https://doi.org/10.1016/j.corsci.2020.108954>
19. Xing BW, Zuo XJ, Li QN, et al (2022) Influence of Microstructure Evolution on the Electrochemical Corrosion Behavior of (CoCrFeNi)<sub>94</sub>Ti<sub>1.5</sub>Al<sub>4.5</sub> High Entropy Alloy Coatings. *J Thermal Spray Technol* 31: 1375–1385. <https://doi.org/10.1007/s11666-022-01364-6>
20. Jin BQ, Zhang NN, Yin S (2022) Strengthening behavior of AlCoCrFeNi(TiN)<sub>x</sub> high-entropy alloy coatings fabricated by plasma spraying and laser remelting. *J Mater Sci Technol* 121:163–173. <https://doi.org/10.1016/j.jmst.2021.12.055>
21. Anupam A, Kottada RS, Kashyap S, et al (2020) Understanding the microstructural evolution of high entropy alloy coatings manufactured by atmospheric plasma spray processing. *Appl Surf Science* 505:144117. <https://doi.org/10.1016/j.apsusc.2019.144117>

## Publisher's Note

Springer Nature remains neutral with regard to jurisdictional claims in published maps and institutional affiliations.